Supplement: Computational Methods and Simulation Details

Mathematical Model

Overview

We constructed a biological process model of the *SHOOT MERISTEMLESS* (*STM*) gene locus to explain our experimental results by expanding a previous mathematical model of a generic polycomb target gene.[1,2] The new model is composed of three main inter-coupled sections, i.e., chromatin histone modification, *STM* expression cycle and DNA replication/cell division (Figure 6A and Figure S6A). The dynamics of H3K27 methylation, demethylation, gene transcription and translation, protein degradation, as well as DNA replication were simulated using the Gillespie's stochastic simulation algorithm (SSA),[3] a classical and widely used method for simulating the stochastic behavior of chemical systems against time evolution by Monte Carlo sampling. This algorithm is defined by a series of possible reactions or events, and a corresponding propensity for each event to occur (master equation). At each iteration, the time interval Δt for the next coming event and the event itself are both selected probabilistically based on Poisson process. Subsequently, the system is updated by performing the selected event, and time is incremented by Δt.

In our simulations, we tracked the methylation status at H3K27, denoted by H_i, of each H3 histone $i \in [1, 2 \ldots, N_{\mathrm{h}}]$ within the *STM* locus on chromatin, where $H_i \in \{\mathrm{me0}, \mathrm{me1}, \mathrm{me2}, \mathrm{me3}\}$ represents the number of methyl group. Here we set $N_{\mathrm{h}} = 36$ to approximate the physical length of *STM* gene (3482 bp) and its promoter, according to the putative value that a nucleosome contains ~200 bp (include linkers). Histones with the indices $2j - 1$ and $2j$, for each positive integer j, were thought to be in the same nucleosome. Meanwhile, we recorded the number of STM protein molecules (actually we did not restrict its values to integers, discuss later), N_{p} in each time step to characterize the *STM* expression level and stem cell fate. Overall, we considered totally $2N_{\mathrm{h}} + 2$ possible events (N_{h} histone methylations, N_{h} histone demethylations, gene expression and protein degradation) in our model. Note that, not all events are possible at any time, e.g., methylation of trimethylated histones or degradation when proteins are no longer presented. The event propensities, which are elaborated in the following text, as denoted by r (with a specific superscript), are recalculated after each system update. Additional information about model parameters is shown in Table S1.

Chromatin Histone Modification

H3K27 methylation. In our model, polycomb repressive complex 2 (PRC2) activity results in the methylation of H3K27 (Figure 6A and S6A). PRC2 is a large protein complex containing an enzymatic subunit with histone methyltransferase activity,[4-7] and a non-catalytic subunit that recognizes H3K27me3/me2.[8] Therefore, PRC2 can recognize existing H3K27me3/me2 and then add methyl group to other histones via a read/write mechanism,[8-10] forming a conserved mechanism in both animals and plants. Meanwhile, both *in vitro* and *in vivo* experimental evidence suggested that PRC2 mostly worked in a non-processive manner,[11,12] adding one methyl group at a time, which we applied in our simulation.

To model H3K27 methylation, we followed the ideas of a previous work,[1] but with slight

differences. Overall, the propensity of methylation, r_i^{me} for histone i, depends on the current methylation status of the surrounding histones, together with some unusual long-range interactions through DNA looping. Besides, r_i^{me} also depends on two reference rates: the PRC2-dependent methylation rate k_{me} and stochastic methylation rate γ_{me}. Moreover, our model also takes the different catalytic abilities of PRC2 on specific methylated substrates (H3K27me0/me1/me2) into account, as supported by *in vitro* experiments.[11] For $1 \le i \le N_{\mathrm{h}}$, the methylation reaction propensities are calculated as

$$\begin{aligned} r_i^{\mathrm{me}} = \beta[&\delta_{H_i,\mathrm{me0}}(\gamma_{\mathrm{me01}} + k_{\mathrm{me01}}E_i) + \\ &\delta_{H_i,\mathrm{me1}}(\gamma_{\mathrm{me12}} + k_{\mathrm{me12}}E_i) + \\ &\delta_{H_i,\mathrm{me2}}(\gamma_{\mathrm{me23}} + k_{\mathrm{me23}}E_i)] \end{aligned} \qquad \text{(Equation S1)}$$

where $\delta_{x,y} = \begin{cases} 1, x = y \\ 0, x \neq y \end{cases}$, is the Kronecker delta symbol.

To incorporate the positive feedback between PRC2 and H3K27me3/me2 (but not H3K27me1), the model allows these two repressive marks to activate PRC2 and promote methylation on neighboring histones.[8] Therefore, we defined an enhancement factor (dimensionless) for histone i, denoted as E_i in Equation S1, to capture this effect

$$E_i = \sum_{j \in M_i \cap [1,\ldots,N_{\mathrm{h}}]} \left(\rho\delta_{H_j,\mathrm{me2}} + \delta_{H_j,\mathrm{me3}}\right) + e_{\mathrm{distal}} \qquad \text{(Equation S2)}$$

where M_i is the neighboring histones, which is defined as

$$M_i = \begin{cases} \{i-3, i-2, i-1, i+1, i+2\}, \text{ if } i \text{ is even} \\ \{i-2, i-1, i+1, i+2, i+3\}, \text{ if } i \text{ is odd} \end{cases} \qquad \text{(Equation S3)}$$

In our model, the first term in Equation S2 accounts for the proximal gain, and ρ represents the reduced efficiency (~10-fold) of activated PRC2 by H3K27me2 relative to H3K27me3.[8] The second term, e_{distal} in Equation S2 captures the contribution of long-range interactions, or distal gain, when DNA looping brings together nucleosomes that are far from each other in one dimension,[13] although this event is less frequent than the others. Note that, in Equation S2, histones outside the *STM* locus are ignored. As a result, this introduces a slight bias toward the active state, especially of histones on boundary nucleosomes, as the boundary histones only undergo one-sided recruitment. However, this bias is expected to be inconsequential.

In this study, we identified that PRC2 can be recruited to *STM* locus by two classes of transcription factor, i.e., *RABBIT EARS* (*RBE*) and *BASIC PENTACYSTEINE* (*BPC*), in a sequence-specific manner. This provides a great example and explanation for the biological background of the relative local PRC2 activity β used in previous models.[1] In our model, β in Equation S1 is understood to be controlled by the polycomb response elements (PREs) and the local activity of RBE/BPC.

H3K27 demethylation. In plants, there exist several demethylases, e.g., jumonji-C domain-containing (JMJD) protein family, that can catalyze H3K27 demethylation.[14,15] Our model applies non-processive demethylation, with one methyl group removal each time. To simplify the model, we no longer considered JMJD alone in the simulation, instead we used a combined demethylation rate, γ_{dem} as the integrated effect of JMJD-dependent and random

removal of methyl groups (Figure 6A and Figure S6A). Therefore, each histone i undergoes demethylation with propensity

$$r_i^{\mathrm{dem}} = \gamma_{\mathrm{dem}}\left(\delta_{H_i,\mathrm{me1}} + \delta_{H_i,\mathrm{me2}} + \delta_{H_i,\mathrm{me3}}\right) \quad \text{(Equation S4)}$$

Furthermore, the model assumes that H3K27 demethylation is also coupled with gene expression event in two ways[1] (Figure 6A and Figure S6A). On one hand, every transcription can result in random histones methylation removal (one methyl groups at a time) at each histone as the RNA polymerase moving,[16] with probability denoted as P_{dem} per histone. Therefore, the process is shown as

$$\text{with probability } [P_{\mathrm{dem}}]\colon H_i \to \begin{cases} \mathrm{me0}, \text{ if } H_i = \mathrm{me1} \\ \mathrm{me1}, \text{ if } H_i = \mathrm{me2} \\ \mathrm{me2}, \text{ if } H_i = \mathrm{me3} \end{cases} \quad \text{(Equation S5)}$$

On the other hand, histone turnover is positively correlated with gene transcriptional activity,[17,18] hence we refreshed each nucleosome (a pair of histones) at each time with exchange probability P_{ex} per histone independently. As a result, the probability that a nucleosome will not be replaced is the product of its two histones, i.e., $(1-P_{\mathrm{ex}})^2$, therefore the turnover process is shown as

$$\text{with probability } [1-(1-P_{\mathrm{ex}})^2]\colon \begin{cases} H_{i-1}/H_i \to \mathrm{me0/me0}, \text{ if } i \text{ is even} \\ H_i/H_{i+1} \to \mathrm{me0/me0}, \text{ if } i \text{ is odd} \end{cases} \quad \text{(Equation S6)}$$

***STM* Expression Cycle**

Gene transcription. *STM* expression, as an important component of our model, is linked to both epigenetic modification and stem cell division (Figure 6A and Figure S6A). Meanwhile, STM protein itself also plays an important role in maintaining the undifferentiated state of pluripotent cells in shoot apical meristem (SAM) and/or axillary meristem (AM).[19,20] To investigate the repressive effect of epigenetic modification on gene transcription, we evaluated the dependence of mRNA production on H3K27me3/me2 levels. The transcriptional initiation rate, f is a piecewise linear function of the average repression level across the *STM* locus, multiplied by another two trans-activation factors (discuss later). Altogether, the formula is given by

$$f = \alpha\theta\left[f_{\max} - \min\left\{\frac{P_{\mathrm{me2/me3}}}{P_T}, 1\right\}\cdot\left(f_{\max} - f_{\min}\right)\right] \quad \text{(Equation S7)}$$

where $f_{\max}$ ($f_{\min}$) is upper (lower) bound and $P_{\mathrm{me2/me3}}$ is the proportion of H3K27me3/me2

$$P_{\mathrm{me2/me3}} = \frac{1}{N_{\mathrm{h}}}\sum_{j=1}^{N_{\mathrm{h}}}\left(\delta_{H_j,\mathrm{me2}} + \delta_{H_j,\mathrm{me3}}\right) \quad \text{(Equation S8)}$$

The threshold, P_T in Equation S7 captures the sub-saturating level for H3K27me3/me2 to reach the maximal repression effect,[21] the rationality of which was justified by fitting mass spectrometry data from stable isotope labeling by amino acids in cell culture (SILAC).[1,22] Moreover, previous model set an upper bound f_{lim} for the transcription initiation rate to restrict it in a reasonable range[1,2]; however, we found that this cannot reproduce all of our experimental results. Instead, we successfully addressed this problem by adding a very low

rate, $\gamma_{\mathrm{transcr}}$ for noisy transcription. Finally, the propensity of *STM* gene transcription is

$$r^{\mathrm{transcr}} = \min\{f, f_{\mathrm{lim}}\} + \gamma_{\mathrm{transcr}} \quad \text{(Equation S9)}$$

In *Arabidopsis*, a previous study revealed a self-sustained loop of *STM* gene in leaf axil to maintain its expression: STM interacts with ATH1, expressed by gene *ARABIDOPSIS THALIANA HOMEOBOX GENE1* (*ATH1*), to form a ATH1-STM complex, subsequently this complex binds to the *STM* locus by ATH1 and activates gene transcription.[23] This process is reminiscent of a ligand-receptor interactions, hence we defined a self-activation factor for this path, denoted as θ in Equation S7, using the Hill equation

$$\theta = \frac{\varepsilon N_{\mathrm{p}}^{\sigma}}{K_d + N_{\mathrm{p}}^{\sigma}} \quad \text{(Equation S10)}$$

where ε, K_d and σ is the maximum self-activation level, apparent disassociation constant and Hill coefficient, respectively. Note that, ε is determined by the affinity between ATH1-STM complex and *STM* locus, thus this parameter actually only varies within a small range, i.e., hardly raises, due to the finite length of *STM* gene and steric effect of binding, although the number of ATH1 protein molecule can be infinite in the system (Figure 7B). Moreover, we set $\sigma > 1$ to reflects the synergistic effect.

In our experiments, we manipulated the cell cycle by overexpressing KRP4/CYCD3;1, both of which could act on cyclin-dependent kinases (CDKs), the key-regulator of cell cycle. KRP4 is a CDK inhibitor (CKI), while CYCD3 can form active complex with CDK4/6.[24] However, CDK activity correlates with stem cell identity maintenance in meristem.[25] Apart from physical dilution effect of epigenetic marks (Figure 5D), in general, we considered two possible molecular pathways, one involving direct action on genes and one involving indirect action on chromatin modification. In our simulation, we took the direct way as major model, while indirect way as alternative model (see Additional Details).

For the direct way, we thought the observed correlation might be explained by *RETINOBLASTOMA-RELATED* (*RBR*), a negative regulator of cell cycle in plants that is inactivated by CDKs.[24] Overexpressing RBR promotes meristem cell differentiation,[26,27] while a reduction in RBR leads to stem cell accumulation and differentiation defect.[26,28] Moreover, transient overexpression of *RBR* decrease the abundance of *Nicotiana tabacum homeobox 15* (*NTH15*, a *KNOX* factor, the ortholog of *Arabidopsis STM*) transcripts in tobacco SAM.[27] During the autotrophic stage of *Arabidopsis*, RBR directly binds to promoters to silence specific genes,[29] but whether *RBR* takes this mechanism or another pathway in meristem is still unclear. However, these results suggest that there do exist a complex regulatory network in meristem. To fit our experimental result and simplify the model, we used the simplest power function to represent the mathematical relationship (net effect, like a compound function) between the two outputs of the network, i.e., division frequency (inverse of cell cycle T) and cycle-dependent *STM* activation factor α

$$\alpha = \max\left\{\left(\frac{T_0}{T}\right)^{\mu}, \alpha_{\mathrm{lim}}\right\} \quad \text{(Equation S11)}$$

where T_0 is the normalized cell cycle, μ is the exponential scaling factor, and α_{lim} is the lower bound, respectively. Besides, previous works suggested that the normal cell cycle in

meristem typically ranged from 18-36 hours,[30,31] and we fixed T_0 to 22.0 hours to follow previous works.[1,2] For biological continuity, if cell cycle changes in our simulations, we introduced a buffering period with a constant exponential changing rate F, therefore the real activation factor α in Equation S7 is given by

$$\alpha = \begin{cases} \max\{\alpha_{\text{old}} e^{-F\Delta t}, \alpha_{\text{new}}\}, & \text{if } \alpha_{\text{new}} < \alpha_{\text{old}} \\ \min\{\alpha_{\text{old}} e^{F\Delta t}, \alpha_{\text{new}}\}, & \text{if } \alpha_{\text{new}} \geq \alpha_{\text{old}} \end{cases} \quad \text{(Equation S12)}$$

where F is positive and α_{old} (α_{new}) is computed from Equation S11 using cell cycle before (after) change, respectively.

In the end, transcription events are coupled with another two events: demethylation and histone exchange, which we have already elaborated above in the section *H3K27 demethylation*.

mRNA translation. To simplify the model, we no longer considered the conversion of the *STM* gene to mRNA (transcription) and of the mRNA to STM protein (translation) as two split processes, instead we combined them into a single step, i.e., gene expression. The purpose of this approach is to eliminate an extra Gillespie's simulation of intermediate state mRNA,[32] which is actually not important in this model mechanism. However, to integrate transcription and translation, we introduced another parameter, n_{ppt} to denote the average protein molecule translated per mRNA transcript (where "ppt" stands for protein per transcription) (Figure 6A and Figure S6A). Once a gene transcription event occurred in the simulation, we added the STM protein number by n_{ppt}. Thus, the protein number in our model is more like a generalized concept, as n_{ppt} can also take float values. Here we ignored the time interval between each translation of the same mRNA transcript.

Protein degradation. In our model, we assumed that the degradation probability was constant. Therefore, the propensity for protein degradation is proportional to the remaining protein molecule number in the system, which is computed as

$$r^{\text{degr}} = \kappa N_{\text{p}} \quad \text{(Equation S13)}$$

where κ is the degradation coefficient. Once a protein degradation event occurred in the simulation, we subtracted the number of STM protein molecule by 1. If the remaining molecule number is less than 1 before subtraction (possibly happen when n_{ppt} is not an integer), then we set it to 0 to avoid generating a negative value.

DNA Replication and Cell Division

In the simulation, DNA replication is inserted into the normal Gillespie process as a truncated event when time of the next coming event exceeds the next replication time.[33] Actually, experiments suggested that H3/H4 tetramers did not dissociate and were shared evenly between daughter strand.[34] Therefore, when replication is carried out, each nucleosome (a pair of histones) is updated with a unmethylated one with a probability of 0.5[1]. After each DNA replication, since we only tracked one daughter strand randomly

$$\text{with probability } [0.5]\text{: } H_{2j-1}/H_{2j} \rightarrow \text{me0/me0} \quad \text{(Equation S14)}$$

Moreover, we performed equal-scaling transformation when cell cycle changed in simulation, e.g., if a cell had 1.5 hours to the next division, and then cell cycle doubled, the transformed cell divided 3 hours later.

Additional Details

Gene activity. Defined as the average transcription number in a cell population per 15 minutes interval.

Cell division arrest. To simulate the situation when cells stop dividing by specific inductor, we allowed the cell cycle to be infinite in our simulations. If cell division is arrested, DNA replication events are excluded from the Gillespie process.

Protein stable/metastable point. According to our model, the propensity for *STM* protein degradation is linear, while the propensity of STM protein production (gene expression) is sigmoid and fluctuates between the two extreme epigenetic state (Figure S6B). For a given situation, the intersections of these two curves represent the fixation points of protein in the ideal system. Regardless, there should be one fixation point (≈0) due to the noisy transcription, which stands for the stably differentiated state (Figure S8, solid blue line). However, the other two fixation points (if both exist) have very different properties. For the larger one, the system reaches a stable equilibrium and tends to recover itself like a spring after perturbation in any direction; thus, we termed this a stable point. Actually, this is the case for normal pluripotent cells with stable *STM* expression (Figure S8, solid red line). For the smaller one, a positive disturbance leads to continuous increase until stable point, which represents the direction of pluripotency restoration, while a negative disturbance causes irreversible decrease until vanish and maintain itself from then on, which represents the direction of differentiation. Altogether, the equilibrium here is unstable and we named it as metastable point, or critical point (Figure S8, green dashed line). When methylation level rises, the stable point drops while the metastable point elevates until they meet at branch point (saddle point) and annihilate, which is similar to saddle-node bifurcation process in mathematics.

Differentiation/pluripotency criteria. We used the remaining number of STM protein molecule in the system to characterize the cell fate. In our simulation, the cells with no STM protein left were viewed as completely differentiated, while the cells with STM protein number more than half of the stable point in the lowest epigenetic repression (H3K27me0) state were viewed as stem cells, others are considered in a transitional state.

Bistability measurement. Bistability (Figure S6C-S6E) describes the ability to maintain both stem cell fate with low histone repression (active transcription) and differentiated cell fate with high histone repression (inactivate transcription) state of *STM* gene. Here we followed the conception of previous models in which the bistability measurement,[1,2,35] B was given by

$$B = 4P_{\mathrm{ON}}P_{\mathrm{OFF}} \qquad \text{(Equation S15)}$$

where P_{ON} stands for the probability of the *STM* gene being in the epigenetic ON state, which is defined as

$$P_{\mathrm{ON}} = \Pr\left(P_{\mathrm{me2/me3}} < \frac{P_T}{4}\right) \qquad \text{(Equation S16)}$$

and likewise, P_{OFF} represents the probability of the *STM* gene being in the epigenetic OFF state

$$P_{\mathrm{OFF}} = \Pr\left(P_{\mathrm{me2/me3}} > \frac{3P_T}{4}\right) \qquad \text{(Equation S17)}$$

In practice, B is calculated using Equation S14 from the combined outputs from the equal number of simulations initiated from either stem cells (uniform H3K27me0, an STM protein level at high stable point) or differentiated cell (uniform H3K27me3, no STM protein). B values closer to 1 indicate stronger bistability. For reliability, we allowed the system to recover from the perturbation of DNA replication before sampling, thus only the data from stable state (last hour of each cell cycle) was used.[1]

Alternative model. As mentioned above, there is another possible pathway in which cell division frequency coupled with histone methylation indirectly affects *STM* transcription. Although the underlying molecular mechanism in plants remains unclear, some studies have suggested that CDK1 could phosphorylate the catalytic subunit of PRC2 at specific target and disrupted its activity in human cells.[36] Therefore, we also proposed an alternative model in which an increase in cell cycle promote PRC2 activity instead of blocking gene transcription directly. In this case, the propensity of histone methylation (Equation S1) and *STM* transcription (Equation S12) are replaced in respective with

$$\begin{aligned} r_i^{\mathrm{me}} = \omega\beta[&\delta_{H_i,\mathrm{me0}}(\gamma_{\mathrm{me01}} + k_{\mathrm{me01}}E_i) + \\ &\delta_{H_i,\mathrm{me1}}(\gamma_{\mathrm{me12}} + k_{\mathrm{me12}}E_i) + \\ &\delta_{H_i,\mathrm{me2}}(\gamma_{\mathrm{me23}} + k_{\mathrm{me23}}E_i)] \end{aligned} \qquad \text{(Equation S1′)}$$

$$f = \theta\left[f_{\max} - \min\left\{\frac{P_{\mathrm{me2/me3}}}{P_T}, 1\right\}\cdot(f_{\max} - f_{\min})\right] \qquad \text{(Equation S7′)}$$

In equation S1′, the cycle-dependent PRC2 activation factor ω is given by simple sigmoid function

$$\omega = \frac{\omega_{\mathrm{lim}}}{1 + e^{-AT+B}} \qquad \text{(Equation S18)}$$

where T is cell cycle, A is the absolute of slope, B is the intercept and ω_{lim} is the upper bound. Here we omitted the buffering period of ω.

Note that, the net effect of both the major/alternative model is decreasing the *STM* transcription efficiency. Thus, as expected, the alternative model gave very similar trajectories of tendency to major model, but with a slower silencing velocity, which is consistent with its indirect manner (Figure 6B-6E, Figure S7A-S7F and Figure S9A-S9H).

Cycle-dependent activation. In major/alternative model, the role of cycle-dependent activation factors, i.e., α and ω, is to alter the fixation point (corresponds to stable state) in system phase space. The dilution of H3K27me3 when DNA replication, in theory, can only change the initial position in the next cycle but not the structure of dynamic system.

Programming Languages and Code Resources

The model programs were written in MATLAB R2024a and Python 3.12. All simulations were tested both on the Windows (win10/win11) and Linux (Ubuntu 20.04/22.04 LTS) operating system. The source code of the model is available at https://github.com/yy420106/stmExpr-chromMod-cellDivModel.

Table S1. Summary of model parameters

Parameter	Biological Description	Value	Notes/References
Global			
N_{h}	Number of H3 histones	36	Fixed by *STM* length
N_{p}	Number of STM protein molecules	$0\sim\infty$	Variable in this study
T	Cell cycle (inverse of cell division frequency) [hour]	$0\sim\infty$	
Gene activation			
T_0	Normalized cell cycle [hour]	22.0	Berry et al.[1] Lövkvist et al.[2] Grandjean et al.[30] Reddy et al.[31]
μ	Power scaling factor	0.5	Free
α_{lim}	Lower bound of cycle-dependent activation factor of *STM*	0.01	
F	Absolute of exponential buffer rate [1/hour]	$\ln 2\,/22.0$	
ε	Maximum self-activation level of *STM*	1.0	
σ	Hill coefficient	2.0	
K_d	Apparent disassociation constant of ATH1-STM complex	180.0	
Gene transcription			
f_{min}	Minimum transcription initiation rate [1/sec]	10^{-4}	Berry et al.[1]
f_{max}	Maximum transcription initiation rate [1/sec]	4×10^{-3}	
f_{lim}	Upper bound of transcription initiation rate [1/sec]	$1/60$	
P_T	Threshold proportion of H3K27me3/me2 marks for maximal repression	$1/3$	Berry et al.[1] Lövkvist et al.[2] Jadhav et al.[21] Alabert et al.[22]
$\gamma_{\mathrm{transcr}}$	Noisy transcription rate [1/sec]	9×10^{-8}	Free
Protein production & degradation			
n_{ppt}	Average proteins translated per mRNA transcript	1.0	Free
κ	Protein degradation rate [1/sec]	4×10^{-6}	Fitted by decay time
Histone methylation			
β	Relative local activity of PRC2 (determined by recruiter RBE/BPC)	1.0	Free
e_{distal}	Distal gain by DNA looping	0.001	
ρ	Reduced efficiency of activated PRC2 between H3K27me2/me3	$1/10$	Berry et al.[1] Lövkvist et al.[2] Margueron et al.[8]
$k_{\mathrm{me23}}(k_{\mathrm{me}})$	PRC2-mediated methylation rate (me2 to me3)	8×10^{-6}	Berry et al.[1]

	[1/sec]		McCabe et al.[11]
k_{me12}	PRC2-mediated methylation rate (me1 to me2) [1/sec]	$6k_{\mathrm{me}}$	
k_{me01}	PRC2-mediated methylation rate (me0 to me1) [1/sec]	$9k_{\mathrm{me}}$	
γ_{me23}	Noisy methylation rate (me2 to me3) [1/sec]	$k_{\mathrm{me23}}/20$	Berry et al.[1] Lövkvist et al.[2]
γ_{me12}	Noisy methylation rate (me1 to me2) [1/sec]	$k_{\mathrm{me12}}/20$	
γ_{me01}	Noisy methylation rate (me0 to me1) [1/sec]	$k_{\mathrm{me01}}/20$	
Histone demethylation			
P_{dem}	Transcription-coupled demethylation probability	5×10^{-3}	Free
P_{ex}	Transcription-coupled per histone exchange probability	1.5×10^{-3}	
γ_{dem}	Integrated demethylation rate [1/sec]	$f_{\mathrm{min}}P_{\mathrm{dem}}$	Berry et al.[1] Lövkvist et al.[2]
Alternative model supplement			
A	Absolute of slope on exponential of sigmoid function	0.5	Free
B	Intercept on exponential of sigmoid function	$11 + \ln 1.5$	
ω_{lim}	Upper bound of cycle-dependent activation factor of PRC2	2.5	

Supplement References

1. Berry, S., Dean, C., and Howard, M. (2017). Slow chromatin dynamics allow Polycomb target genes to filter fluctuations in transcription factor activity. Cell Syst *4*, 445-457.e448. 10.1016/j.cels.2017.02.013.
2. Lövkvist, C., Mikulski, P., Reeck, S., Hartley, M., Dean, C., and Howard, M. (2021). Hybrid protein assembly-histone modification mechanism for PRC2-based epigenetic switching and memory. eLife *10*, e66454. 10.7554/eLife.66454.
3. Gillespie, D.T. (1977). Exact stochastic simulation of coupled chemical reactions. The Journal of Physical Chemistry *81*, 2340-2361. 10.1021/j100540a008.
4. Goodrich, J., Puangsomlee, P., Martin, M., Long, D., Meyerowitz, E.M., and Coupland, G. (1997). A Polycomb-group gene regulates homeotic gene expression in *Arabidopsis*. Nature *386*, 44-51. 10.1038/386044a0.
5. Czermin, B., Melfi, R., McCabe, D., Seitz, V., Imhof, A., and Pirrotta, V. (2002). Drosophila enhancer of Zeste/ESC complexes have a histone H3 methyltransferase activity that marks chromosomal Polycomb sites. Cell *111*, 185-196. 10.1016/s0092-8674(02)00975-3.
6. Müller, J., Hart, C.M., Francis, N.J., Vargas, M.L., Sengupta, A., Wild, B., Miller, E.L., O'Connor, M.B., Kingston, R.E., and Simon, J.A. (2002). Histone methyltransferase activity of a Drosophila Polycomb group repressor complex. Cell *111*, 197-208. 10.1016/s0092-8674(02)00976-5.
7. Chanvivattana, Y., Bishopp, A., Schubert, D., Stock, C., Moon, Y.H., Sung, Z.R., and Goodrich, J. (2004). Interaction of Polycomb-group proteins controlling flowering in Arabidopsis. Development (Cambridge, England) *131*, 5263-5276. 10.1242/dev.01400.
8. Margueron, R., Justin, N., Ohno, K., Sharpe, M.L., Son, J., Drury, W.J., 3rd, Voigt, P., Martin, S.R., Taylor, W.R., De Marco, V., et al. (2009). Role of the polycomb protein EED in the propagation of repressive histone marks. Nature *461*, 762-767. 10.1038/nature08398.
9. Schubert, D., Primavesi, L., Bishopp, A., Roberts, G., Doonan, J., Jenuwein, T., and Goodrich, J. (2006). Silencing by plant Polycomb-group genes requires dispersed trimethylation of histone H3 at lysine 27. EMBO J *25*, 4638-4649. 10.1038/sj.emboj.7601311.
10. Hansen, K.H., Bracken, A.P., Pasini, D., Dietrich, N., Gehani, S.S., Monrad, A., Rappsilber, J., Lerdrup, M., and Helin, K. (2008). A model for transmission of the H3K27me3 epigenetic mark. Nature cell biology *10*, 1291-1300. 10.1038/ncb1787.
11. McCabe, M.T., Graves, A.P., Ganji, G., Diaz, E., Halsey, W.S., Jiang, Y., Smitheman, K.N., Ott, H.M., Pappalardi, M.B., Allen, K.E., et al. (2012). Mutation of A677 in histone methyltransferase EZH2 in human B-cell lymphoma promotes hypertrimethylation of histone H3 on lysine 27 (H3K27). Proceedings of the National Academy of Sciences of the United States of America *109*, 2989-2994. 10.1073/pnas.1116418109.
12. Zee, B.M., Britton, L.M., Wolle, D., Haberman, D.M., and Garcia, B.A. (2012). Origins and formation of histone methylation across the human cell cycle. Molecular and cellular biology *32*, 2503-2514. 10.1128/mcb.06673-11.
13. Ogiyama, Y., Schuettengruber, B., Papadopoulos, G.L., Chang, J.M., and Cavalli, G. (2018). Polycomb-Dependent Chromatin Looping Contributes to Gene Silencing during Drosophila Development. Molecular cell *71*, 73-88.e75. 10.1016/j.molcel.2018.05.032.

14. Lu, F., Cui, X., Zhang, S., Jenuwein, T., and Cao, X. (2011). Arabidopsis REF6 is a histone H3 lysine 27 demethylase. Nature genetics *43*, 715-719. 10.1038/ng.854.
15. Zheng, S., Hu, H., Ren, H., Yang, Z., Qiu, Q., Qi, W., Liu, X., Chen, X., Cui, X., Li, S., et al. (2019). The Arabidopsis H3K27me3 demethylase JUMONJI 13 is a temperature and photoperiod dependent flowering repressor. Nat Commun *10*, 1303. 10.1038/s41467-019-09310-x.
16. Chen, S., Ma, J., Wu, F., Xiong, L.J., Ma, H., Xu, W., Lv, R., Li, X., Villen, J., Gygi, S.P., et al. (2012). The histone H3 Lys 27 demethylase JMJD3 regulates gene expression by impacting transcriptional elongation. Genes & development *26*, 1364-1375. 10.1101/gad.186056.111.
17. Deaton, A.M., Gómez-Rodríguez, M., Mieczkowski, J., Tolstorukov, M.Y., Kundu, S., Sadreyev, R.I., Jansen, L.E., and Kingston, R.E. (2016). Enhancer regions show high histone H3.3 turnover that changes during differentiation. Elife *5*. 10.7554/eLife.15316.
18. Kraushaar, D.C., Jin, W., Maunakea, A., Abraham, B., Ha, M., and Zhao, K. (2013). Genome-wide incorporation dynamics reveal distinct categories of turnover for the histone variant H3.3. Genome biology *14*, R121. 10.1186/gb-2013-14-10-r121.
19. Long, J.A., and Barton, M.K. (1998). The development of apical embryonic pattern in *Arabidopsis*. Development *125*, 3027-3035.
20. Long, J., and Barton, M.K. (2000). Initiation of axillary and floral meristems in *Arabidopsis*. Dev Biol *218*, 341-353. 10.1006/dbio.1999.9572.
21. Jadhav, U., Manieri, E., Nalapareddy, K., Madha, S., Chakrabarti, S., Wucherpfennig, K., Barefoot, M., and Shivdasani, R.A. (2020). Replicational Dilution of H3K27me3 in Mammalian Cells and the Role of Poised Promoters. Molecular Cell *78*, 141-151.e145. 10.1016/j.molcel.2020.01.017.
22. Alabert, C., Barth, T.K., Reverón-Gómez, N., Sidoli, S., Schmidt, A., Jensen, O.N., Imhof, A., and Groth, A. (2015). Two distinct modes for propagation of histone PTMs across the cell cycle. Genes & development *29*, 585-590. 10.1101/gad.256354.114.
23. Cao, X., Wang, J., Xiong, Y., Yang, H., Yang, M., Ye, P., Bencivenga, S., Sablowski, R., and Jiao, Y. (2020). A self-activation loop maintains meristematic cell fate for branching. Curr Biol *30*, 1893-1904.e1894. 10.1016/j.cub.2020.03.031.
24. Inzé, D., and De Veylder, L. (2006). Cell cycle regulation in plant development. Annual review of genetics *40*, 77-105. 10.1146/annurev.genet.40.110405.090431.
25. Gaamouche, T., Manes, C.L., Kwiatkowska, D., Berckmans, B., Koumproglou, R., Maes, S., Beeckman, T., Vernoux, T., Doonan, J.H., Traas, J., et al. (2010). Cyclin-dependent kinase activity maintains the shoot apical meristem cells in an undifferentiated state. Plant J *64*, 26-37. 10.1111/j.1365-313X.2010.04317.x.
26. Wildwater, M., Campilho, A., Perez-Perez, J.M., Heidstra, R., Blilou, I., Korthout, H., Chatterjee, J., Mariconti, L., Gruissem, W., and Scheres, B. (2005). The *RETINOBLASTOMA-RELATED* gene regulates stem cell maintenance in *Arabidopsis* roots. Cell *123*, 1337-1349. 10.1016/j.cell.2005.09.042.
27. Wyrzykowska, J., Schorderet, M., Pien, S., Gruissem, W., and Fleming, A.J. (2006). Induction of differentiation in the shoot apical meristem by transient overexpression of a retinoblastoma-related protein. Plant physiology *141*, 1338-1348. 10.1104/pp.106.083022.
28. Borghi, L., Gutzat, R., Fütterer, J., Laizet, Y., Hennig, L., and Gruissem, W. (2010). *Arabidopsis*

RETINOBLASTOMA-RELATED is required for stem cell maintenance, cell differentiation, and lateral organ production. Plant Cell *22*, 1792-1811. 10.1105/tpc.110.074591.

29. Gutzat, R., Borghi, L., Fütterer, J., Bischof, S., Laizet, Y., Hennig, L., Feil, R., Lunn, J., and Gruissem, W. (2011). RETINOBLASTOMA-RELATED PROTEIN controls the transition to autotrophic plant development. Development (Cambridge, England) *138*, 2977-2986. 10.1242/dev.060830.
30. Grandjean, O., Vernoux, T., Laufs, P., Belcram, K., Mizukami, Y., and Traas, J. (2004). *In vivo* analysis of cell division, cell growth, and differentiation at the shoot apical meristem in *Arabidopsis*. Plant Cell *16*, 74-87. 10.1105/tpc.017962.
31. Reddy, G.V., Heisler, M.G., Ehrhardt, D.W., and Meyerowitz, E.M. (2004). Real-time lineage analysis reveals oriented cell divisions associated with morphogenesis at the shoot apex of *Arabidopsis thaliana*. Development *131*, 4225-4237. 10.1242/dev.01261.
32. Ozbudak, E.M., Thattai, M., Kurtser, I., Grossman, A.D., and van Oudenaarden, A. (2002). Regulation of noise in the expression of a single gene. Nature genetics *31*, 69-73. 10.1038/ng869.
33. Bratsun, D., Volfson, D., Tsimring, L.S., and Hasty, J. (2005). Delay-induced stochastic oscillations in gene regulation. Proceedings of the National Academy of Sciences of the United States of America *102*, 14593-14598. 10.1073/pnas.0503858102.
34. Annunziato, A.T. (2005). Split decision: what happens to nucleosomes during DNA replication? The Journal of biological chemistry *280*, 12065-12068. 10.1074/jbc.R400039200.
35. Sneppen, K., and Dodd, I.B. (2012). A simple histone code opens many paths to epigenetics. PLoS computational biology *8*, e1002643. 10.1371/journal.pcbi.1002643.
36. Wei, Y., Chen, Y.H., Li, L.Y., Lang, J., Yeh, S.P., Shi, B., Yang, C.C., Yang, J.Y., Lin, C.Y., Lai, C.C., and Hung, M.C. (2011). CDK1-dependent phosphorylation of EZH2 suppresses methylation of H3K27 and promotes osteogenic differentiation of human mesenchymal stem cells. Nature cell biology *13*, 87-94. 10.1038/ncb2139.

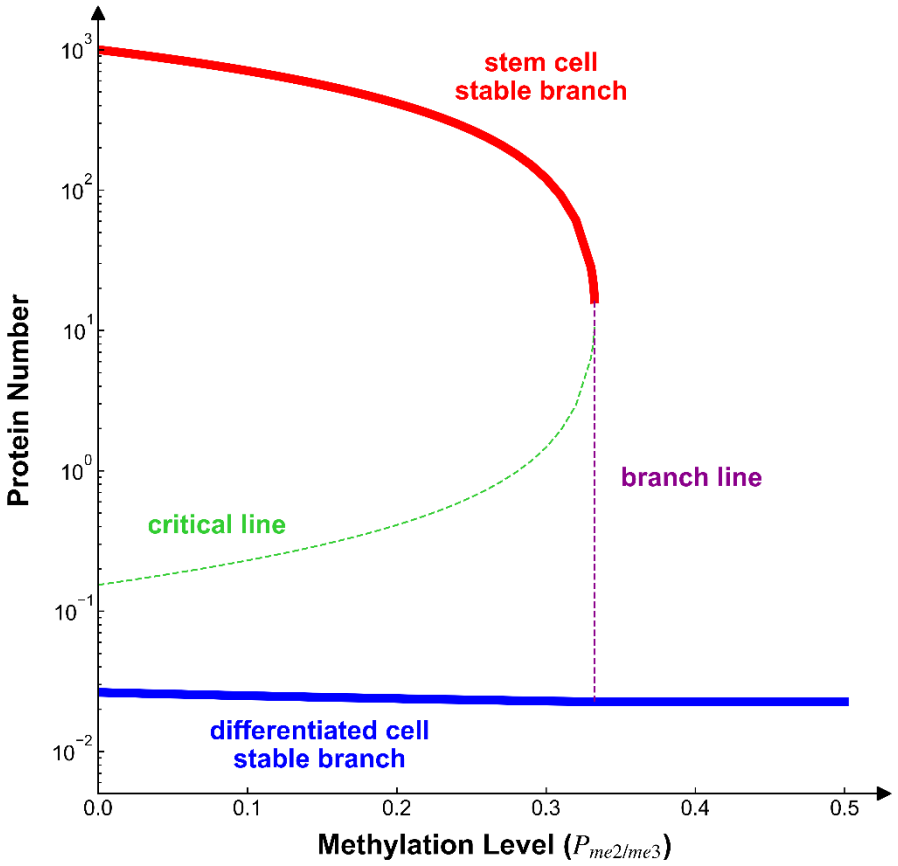

Figure S8. Cell fate bifurcation in model phase space

Solid blue line represents the stable branch of fully differentiated cells. Solid red line represents the stable branch of stem cells, that annihilates at the left limit of branch line (purple dashed line). Green dashed line represents the trajectory of critical/metastable point, which divide the left space into pluripotency bias and differentiation bias region.

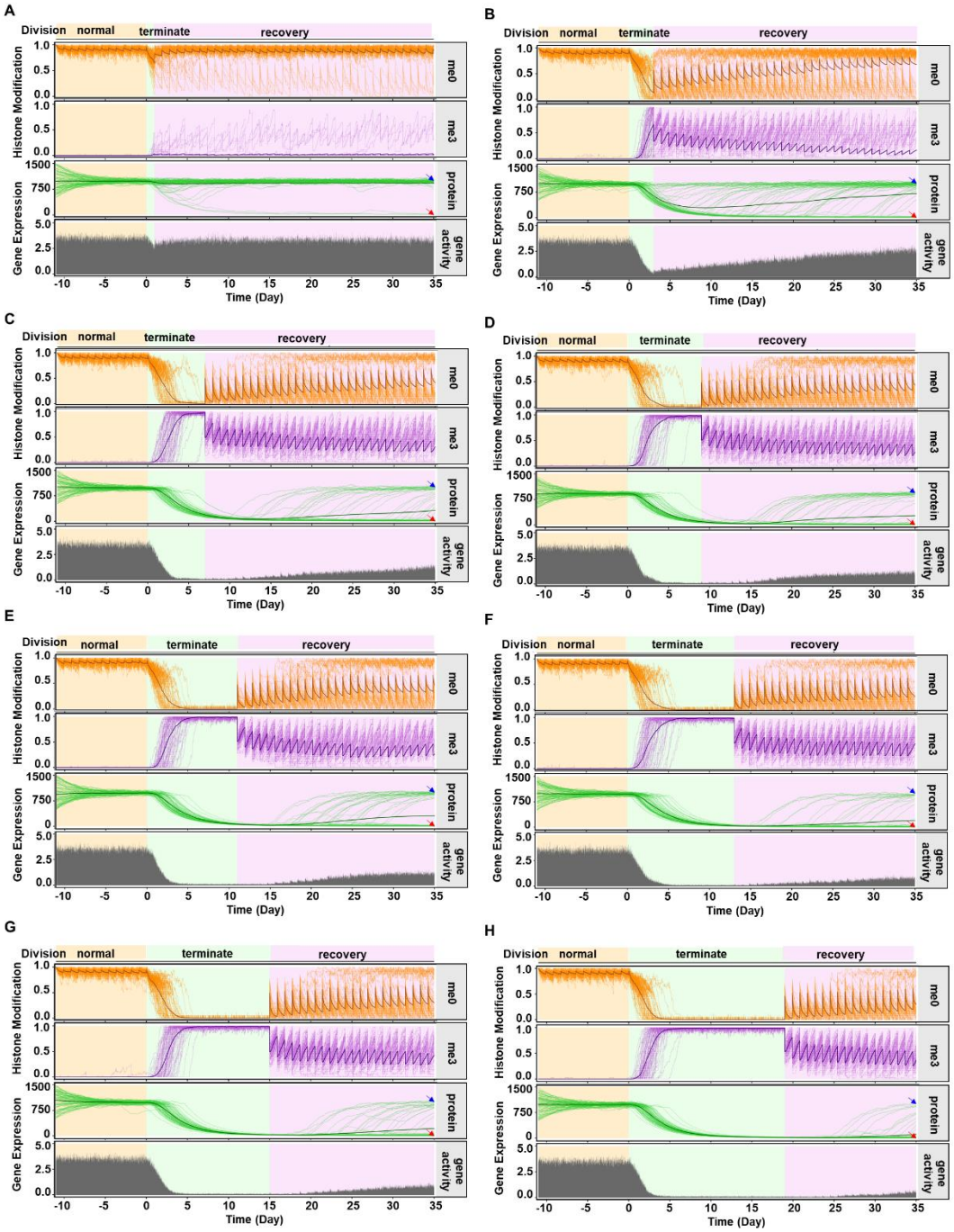

Figure S9. Prediction of alternative model

(A-H) Representative trajectories from stochastic simulations of (A) 1 day, (B) 3 days, (C) 7 days, (D) 9 days, (E) 11 days, (F) 13 days, (G) 15 days and (H) 19 days cell division arrest treatment before recovery using the alternative model, in which cell division frequency affects PRC2 activity instead. Simulations were started randomly from ±50% fluctuation of protein stable points in stem cell (uniform H3K27me0) with normal cell cycle (22.0 h), and performed 12 cell cycle for pre-equilibrium before quiescence. Each graph shows 80 overplotted

trajectories. Histone modification level averaged within *STM* locus. Heavy line in each panel represents the average curve of the cell population. Red arrowhead, differentiated group; blue arrowhead, stem-restored group. Gene activity measured as the average number of transcription events in cell population per 15 min interval. Other parameters are fixed to their default values, as listed in Table S1. See also Figure 6B-6E and Figure S7A-S7F.